AGO1 regulates pericentromeric regions in mouse embryonic stem cells

Madlen Müller[1,2], Tara Fäh[1], Moritz Schaefer[1,2], Victoria Hermes[1], Janina Luitz[1], Patrick Stalder[1,2], Rajika Arora[1], Richard Patryk Ngondo[1, £] and Constance Ciaudo[1, *].

[1] Swiss Federal Institute of Technology Zurich, IMHS, Chair of RNAi and Genome Integrity, Zurich, Switzerland.

[2] Life Science Zurich Graduate School, University of Zürich, Switzerland.

[£] Current address: Institut de Biologie Moléculaire des Plantes UPR-CNRS 2357, Strasbourg, France.

* Correspondence: cciaudo@ethz.ch

Running title: AGO1 regulates heterochromatin localization

Key words: AGO1, H3K9me3, HP1α, major satellites, miR-30, pericentromeres.

Summary blurb

Depletion of AGO1 in mESCs leads to a redistribution of H3K9me3 and HP1α away from pericentromeric regions and is accompanied by an upregulation of major satellites transcripts.

ABSTRACT

Argonaute proteins (AGOs), that play an essential role in cytosolic post-transcriptional gene silencing, have been also reported to function in nuclear processes like transcriptional activation or repression, alternative splicing and, chromatin organization. As most of these studies have been conducted in human cancer cell lines, the relevance of AGOs nuclear functions in the context of mouse early embryonic development remains uninvestigated. Here, we examined a possible role of the AGO1 protein on the distribution of constitutive heterochromatin in mouse Embryonic Stem Cells (mESCs). We observed a specific redistribution of the repressive histone mark H3K9me3 and the heterochromatin protein HP1α, away from pericentromeric regions upon *Ago1* depletion. Furthermore, we demonstrated that major satellite transcripts are strongly upregulated in *Ago1*_KO mESCs and that their levels are partially restored upon AGO1 rescue. We also observed a similar redistribution of H3K9me3 and HP1α in *Drosha*_KO mESCs, suggesting a role for microRNAs (miRNAs) in the regulation of heterochromatin distribution in mESCs. Finally, we showed that specific miRNAs with complementarity to major satellites can partially regulate the expression of these transcripts.

INTRODUCTION

The microRNA (miRNA) pathway is crucial in regulating early embryonic development and differentiation *in vivo* and *in vitro* (DeVeale *et al*, 2021). MiRNAs can fine-tune gene expression throughout early embryonic development at the post-transcriptional level. MiRNA precursors are processed into ~22 nt long mature miRNAs by two consecutive cleavage steps conducted by the RNAse III enzyme DROSHA in the nucleus, and DICER, in the cytoplasm (Bodak *et al*, 2017). Mature miRNAs are loaded into Argonaute (AGO) proteins, which are key components of the RNA-Induced Silencing Complex (RISC). They guide the RISC complex to partially complementary target sequences leading to the translational inhibition of these targets (Bartel, 2018).

In mice, there are four AGO proteins (AGO1-4), but only AGO1 and AGO2 are detectably expressed during early embryonic development, with AGO2 being substantially more abundant (Lykke-Andersen *et al*, 2008; Boroviak *et al*, 2018; Müller *et al*, 2020). While *Ago2* deficient mice die at a post-implantation stage, due to severe developmental defects (Liu *et al*, 2004; Alisch *et al*, 2007; Morita *et al*, 2007; Cheloufi *et al*, 2010), *Ago1,3,4* deficient mice are viable (Modzelewski *et al*, 2012; Van Stry *et al*, 2012).

Mouse Embryonic Stem Cells (mESCs), which are derived from the inner cell mass of the blastocyst, are a powerful tool to study early embryonic development *in vitro.* These cells are pluripotent and can differentiate into the three embryonic germ layers. As observed *in vivo*, mESCs only express AGO1 and AGO2 proteins (Lykke-Andersen *et al*, 2008; Boroviak *et al*, 2018; Müller *et al*, 2020). MESCs deficient for either AGO1 or AGO2 are viable, can exit from pluripotency and differentiate into the three embryonic germ layers (Ngondo *et al*, 2018).

In addition to their major role in the cytoplasmic miRNA pathway, several studies have reported noncanonical functions of the AGO proteins in the nucleus (Meister, 2013; Gagnon *et al*, 2014a; Li *et al*, 2020). AGO2 was shown to shuttle into the nucleus with the help of TNRC6A (Nishi *et al*, 2013). In the nucleus, guided by small RNAs (smRNAs), both AGO1 and AGO2 have been shown to localize to promoter regions and reinforce the recruitment of chromatin modifiers leading to either transcriptional activation or silencing (Janowski *et al*, 2006; Kim *et al*, 2006; Li *et al*, 2006; Hu *et al*, 2012; Cho *et al*, 2014; Portnoy *et al*, 2016). AGO1 was also found to be enriched at promoters of actively transcribed genes, where it interacts with RNA Polymerase II (RNA PolII) (Huang *et al*, 2013). Furthermore, AGO1 was found to localize to enhancer regions, which was dependent on a species of RNA called enhancer RNAs (eRNAs) (Alló *et al*, 2014; Shuaib *et al*, 2019). Additionally, interaction of AGO1 with enhancers was shown to be crucial for maintenance of 3D chromatin organization and more recently to control myogenic differentiation (Shuaib *et al*, 2019;

Fallatah *et al*, 2021). Finally, AGO1 has been implicated in alternative splicing events, taking place within the nucleus (Ameyar-Zazoua *et al*, 2012; Agirre *et al*, 2015; Alló *et al*, 2014). Of note, most of these chromatin-associated functions have been described mainly for AGO1, while AGO2 was reported to be involved in double strand break repair (Gao *et al*, 2014; Wang & Goldstein, 2016).

Most of the aforementioned AGOs functions were described in human cancer cell lines and have not been studied during early embryonic development. Only few studies reported phenotypes associating the AGO proteins with other functions in mESCs (Sarshad *et al*, 2018; Kelly *et al*, 2019; Shivram *et al*, 2019). For instance, Kelly et al., identified that TGF-β pathway targets are upregulated upon AGO2 depletion in mESCs, due to a lack of miRNA repression. The upregulation of these targets additionally correlated with decreased levels of the repressive histone mark, H3K27me3 (Kelly *et al*, 2019). Interestingly, we also observed a specific loss of H3K27me3 mark in *Ago1&2*_KO mESCs (Mueller *et al*, 2021). Repressive histone marks are important for the formation of heterochromatin, which is localized to distinct territories within the nucleus (Solovei *et al*, 2009; Akhtar & Gasser, 2007).

In this study, we aimed to explore the link between AGO1 and heterochromatin by assessing both the amount and the distribution of constitutive heterochromatin in *Ago1* mutant mESCs. We observed a specific redistribution of the repressive histone mark H3K9me3 and, the heterochromatin protein HP1α away from pericentromeric regions in *Ago1*_KO mESCs. Furthermore, these regions are characterized by AT-rich tandem repeats known as major satellite sequences. We demonstrated that major satellite transcripts are strongly upregulated in *Ago1*_KO mESCs. Nevertheless, we did not observe any changes in integrity of the pericentromeric region at the DNA level. Importantly, these phenotypes were rescued upon the reintroduction of AGO1 in the mutant cells. These results prompted us to investigate the underlying molecular mechanism by which AGO1 might regulate major satellite transcripts. We first demonstrated the involvement of miRNAs by observing a similar redistribution of H3K9me3 and HP1α in *Drosha*_KO mESCs. Using computational analyses and molecular approaches, we also found that AGO1, loaded with miR-30a, d, e-3p, might contribute partially to the regulation of major satellite transcripts. Overall, our results demonstrate for the first time a novel role for AGO1 in regulating major satellite transcripts and localization of H3K9me3 and HP1α at pericentromeres in mESCs.

RESULTS

Ago1 depletion affects the distribution of H3K9me3 and HP1α at pericentromeric regions

Only the H3K27me3 heterochromatin mark, but not H3K9me3, was previously observed to be strongly downregulated in Argonaute mutant mESCs (Kelly *et al*, 2019; Mueller *et al*, 2021). Heterochromatin is localized to specific nuclear territories in mammalian cells (Solovei *et al*, 2009; Akhtar & Gasser, 2007). H3K9me3, in particular, is enriched at pericentromeric constitutive heterochromatin regions in mammals, which can be found at the centromeres. Constitutive heterochromatin at centromeres is required for proper sister chromatid cohesion and chromosome segregation (Guenatri *et al*, 2004; Probst & Almouzni, 2008; Bernard *et al*, 2001; Houlard *et al*, 2006; Nonaka *et al*, 2002; Probst *et al*, 2009). Pericentromeric domains from several chromosomes are known to cluster together within interphase in order to form chromocenters (Guenatri *et al*, 2004; Probst & Almouzni, 2008). Chromocenters are easily visible by fluorescence microscopy with a brighter DAPI stain (Guenatri *et al*, 2004; Probst & Almouzni, 2008). AGO1 has been previously linked to chromatin associated functions in mammalian cells (Alló et al., 2014; Huang et al., 2013; Shuaib et al., 2019). In order to study whether AGO1 might be important for constitutive heterochromatin localization in mESCs, we used two *Ago1*_KO mESC lines generated using a paired CRISPR-Cas9 approach (Wettstein *et al*, 2016). The first *Ago1*_KO1 mESC line was obtained from a previous study (Ngondo *et al*, 2018) and the second *Ago1*_KO2 mESCs line was newly generated and validated for the absence of AGO1 expression (Fig S1A and B). As previously observed in *Ago1&2*_KO mESCs (Mueller *et al*, 2021), the total amount of H3K9me3 histone mark as assessed by western blotting (WB) was similar in WT versus *Ago1*_KO mESCs (Fig S1C). To go further, we analyzed the nuclear localization of H3K9me3 by indirect Immunofluorescence (IF) and observed colocalization of H3K9me3 with DAPI rich regions in WT mESCs (Fig 1A, S1D). Surprisingly, this colocalization of H3K9me3 with DAPI rich regions, was strongly reduced in *Ago1*_KO mESCs (Fig 1A).

To strengthen these observations, we performed H3K9me3 Chromatin Immunoprecipitation followed by quantitative PCR (ChIP-qPCR) in WT versus *Ago1*_KO mESCs and successfully assessed the enrichment at known heterochromatic loci (Karimi *et al*, 2011; Ngondo *et al*, 2018) over a control region (Fig S1E and Table S1). We also compared the H3K9me3 enrichment at major satellites sequences in both WT and *Ago1*_KO, and observed that upon *Ago1* depletion, around 50% of H3K9me3 is lost at these sites (Fig 1B and Table S1).

H3K9me3 is deposited at pericentromeric heterochromatin regions by the methyltransferase SUV39H1/2, which is recruited there by HP1α (also known as CBX5) (Lachner *et al*, 2001; Bannister *et al*, 2001; Hyun *et al*, 2017). Therefore, we assessed the colocalization of HP1α

with DAPI rich regions in WT and *Ago1*_KO mESCs by IF (Fig 1C). Similarly, we observed a significant redistribution of HP1α in *Ago1*_KO mESCs, away from the pericentromeric regions (Fig 1C). In addition, we noted a slight increase of HP1α protein expression in *Ago1*_KO mESCs compared to WT cells (Fig S1F).

In conclusion, we observed a redistribution of both the repressive histone mark H3K9me3 and the heterochromatin protein HP1α, away from pericentromeric regions in *Ago1*_KO mESCs.

AGO1 complementation rescues the distribution of H3K9me3 and HP1α at pericentromeric regions

In order to determine, whether the redistribution of H3K9me3 away from pericentromeric regions is specific to the loss of AGO1, we aimed to complement our *Ago1*_KO mESCs. We transfected the *Ago1*_KO2 mESC line with a vector expressing N-terminally HA-tagged AGO1. This vector additionally contains two selection markers, a GFP and a puromycin resistance gene. Cells expressing AGO1 were selected for a week for puromycin resistance, followed by FACS sorting for GFP (Fig S2A). Finally, we verified HA-AGO1 expression in the GFP sorted polyclonal cell population (mixed cell population) by IF and WB, and observed a partial rescue of AGO1 levels in the complemented cells (Fig 2A and S2B). We next tested whether the reintroduction of AGO1 could rescue the distribution of H3K9me3 foci at DAPI rich regions and performed a co-staining for H3K9me3 and HA in WT, *Ago1*_KO and the *Ago1*_KO + HA-AGO1 cells (Fig 2A). The co-staining with HA allowed us to select cells re-expressing AGO1 at a proper level in the polyclonal population to perform the quantification. We observed a significant rescue of the H3K9me3 distribution at the pericentromeric regions upon reintroduction of AGO1 in *Ago1*_KO mESC line (Fig 2A).

Due to the nuclear pre-extraction step necessary for proper visualization of HP1α by IF, we were not able to simultaneously assess the distribution of HP1α along with HA-AGO1 in the complemented polyclonal population. To solve this issue, we selected monoclonal clones using GFP as a marker by FACS sorting (Fig S2C). Two clones (B2 and A9) were kept for further analysis as they expressed HA-AGO1 at similar (B2) or at a higher level (A9) than the complemented polyclonal population of cells previously analyzed (Fig S2D). We then assessed the distribution of HP1α in WT, *Ago1*_KO and *Ago1*_KO complemented clones by IF and, observed a similar significant rescue of the HP1α distribution at the pericentromeres upon reintroduction of AGO1 in *Ago1*_KO mESC single clones (Fig 2B).

In conclusion, the reintroduction of AGO1 in *Ago1*_KO mESCs partially rescue the mislocalization of both H3K9me3 and HP1α at pericentromeres.

Major satellite transcripts are upregulated in *Ago1*_KO mESCs

In mouse, pericentromeric heterochromatin regions are characterized by AT-rich tandem repeats, known as major satellite repeat sequences. Major satellites consist of 234 bp tandem repeat sequences that can stretch over several kilobases (Komissarov *et al*, 2011; Guenatri *et al*, 2004). The minor satellite sequences adjacent to the major satellites are localized to the centromeric part of the chromosome (Fig S3A) (Vissel & Choo, 1989; Guenatri *et al*, 2004). Even though pericentromeric regions are marked by repressive heterochromatin marks, pericentromeric transcripts, such as major satellite transcripts, have been previously reported to be expressed *in vivo* during mouse early development and also *in vitro* in mESCs (Fig S3A) (Rudert *et al*, 1995; Lehnertz *et al*, 2003; Probst *et al*, 2010).

In order to assess whether the depletion of *Ago1* affects major satellite transcripts, we performed an RNA Fluorescent *In Situ* Hybridization (FISH) (Fig 3A). We observed a stronger signal and significantly more foci corresponding to major satellites in *Ago1*_KO compared to WT mESCs (Fig 3A and S3A). To confirm that the increase in foci number per cell corresponding to transcripts derived from major satellites is specific to the loss of AGO1 in mESCs, we performed RNA FISH in the previously derived single complemented clones A9 and B2. We observed that the reintroduction of AGO1 in *Ago1*_KO mESCs could also partially rescue the RNA FISH signal in the single complemented clones (Fig 3A). To better quantify the amount of major satellite transcripts in all cell lines, we then measured their relative expression using a stringent RT-qPCR protocol in WT, *Ago1*_KO and Ago1_KO complemented clones (see Materials and Methods and Fig S3B). We detected a significant upregulation of major satellite mRNAs in the *Ago1*_KO mESCs using two independent primer pairs and this upregulation was decreased by half upon reintroduction of AGO1 in *Ago1*_KO mESC clones (Fig 3B).

Finally, to better understand whether the upregulation of major satellite transcripts was linked to changes at the chromatin level, we analyzed the IF images for the H3K9me3 staining and quantified the number of DAPI foci (chromocenters) in WT versus *Ago1*_KO mESCs. We observed no decrease of DAPI foci formation in *Ago1*_KO compared to WT mESCs (Fig S3C). Additionally, we also performed DNA FISH for the major satellite repeats in these two cell lines. The major satellite DNA FISH signal was similar between WT and *Ago1*_KO mESCs and we did not detect a more dispersed signal for the major satellites in *Ago1*_KO mESCs, indicating that the overall structures of chromocenters is preserved in *Ago1*_KO mESCs (Fig S3D).

In summary, we observed that upon *Ago1* depletion, major satellite transcripts are upregulated in mESCs and that their expression can be partially rescued by the re-expression of AGO1. Furthermore, this phenotype was not accompanied by the loss of chromocenters structure, as they could still form normally in *Ago1*_KO mESCs.

MiRNAs are involved in the regulation of major satellites in mESCs

We then attempted to identify the molecular mechanism causing the upregulation of major satellite transcripts in *Ago1*_KO mESCs. The AGO proteins are best known for their role in post-transcriptional silencing via miRNAs (Meister, 2013). In order to investigate the role of miRNAs in constitutive heterochromatin distribution in mESCs, we performed IF of H3K9me3 and HP1α in *Drosha*_KO mESCs (Cirera-Salinas *et al*, 2017), generated in the same background than our *Ago1*_KO mESCs. Interestingly, we observed a strong redistribution of H3K9me3 and HP1α away from the pericentromeric regions in *Drosha*_KO compared to WT mESCs, suggesting a role for miRNAs in the regulation of pericentromeric regions in mESCs (Fig 4A and B). Additionally, we observed an upregulation of HP1α in *Drosha*_KO mESCs (Fig S4A), suggesting that HP1α itself might be directly regulated by miRNAs.

MiRNA gene regulation is usually taking place in the cytoplasm of the cells (Bartel, 2018). Nevertheless, AGO2 was previously shown to shuttle into the nucleus (Nishi *et al*, 2013) and be enriched in mESC nucleus (Sarshad *et al*, 2018). Accordingly, we sought to assess the subcellular distribution of AGO1 in mESCs. Using well established biochemical assays (Gagnon *et al*, 2014b), we performed cytoplasmic/nucleoplasmic/chromatin fractionation of WT mESCs and analyzed the abundance of AGO1 in these three fractions by WB (Fig 4C). We observed that the majority of AGO1 localized to the cytoplasm, whereas only around 10-15% of AGO1 is present in the nuclear fraction and even less than 3% is found in the chromatin fraction (Fig 4C). Cross-contamination was controlled for by using specific subcellular markers to validate the purity of the different fractions (Fig 4C). These results led us to hypothesize that, like AGO2, AGO1 loaded with miRNA is able to shuttle in the nucleus of mESCs and might target specific transcripts in the nucleus. We therefore attempted to identify whether miRNAs target major satellite transcripts in mESCs. Most major satellite annotations, as obtained from RepeatMasker and Dfam (Smit *et al*; Storer *et al*, 2021; Bao *et al*, 2015), were not properly mapped to any of the chromosomes and therefore annotated in unmapped genomic contigs (Fig S4B). In accordance with reports of major satellite sequences being several kilobases long, we selected those annotations that mapped to regions of at least 20 kbps of length, and focused on major satellite regions that mapped to chromosome X, 9 and the contigs JH583204.1 and GL456383.1. We searched for miRNAs with high confidence seed matches within these sequences and identified three miRNAs from the miR-30 family having a high number (more than 500) of 8mer binding sites (BS) within major satellite sequences (Fig 4D). Additionally, two other miRNAs miR-139-5p and mR-6989-3p showed significant predicted BS. However, both these had much fewer binding

sites compared to the miR-30-3p family (Fig 4D). Whereas, miR-139-5p has around 200 BS for the annotated region on the X chromosome, it has basically no BS for the other three regions. Also, miR-6989-3p has only around 100 BS in two contigs and even less in the others (Fig 4D).

The miR-30 family is composed of 6 pre-miRNAs, (miR-30a, miR-30b, miR-30c-1, miR-30c-2, miR-30d, miR-30e) located on three different chromosomes, which are all expressed in WT mESCs (Fig S4C and D, Table S2). While all the mature miR-30-5p share the same seed sequence, only miR-30a-3p, miR-30d-3p and miR-30e-3p have identical seeds, which match the major satellite sequences (Fig 4D and S4E). Additionally, by re-analyzing our published AGO1 RNA immunoprecipitation and sequencing (RIP-seq) data (Ngondo *et al*, 2018), we identified that these three miRNAs are preferentially loaded into AGO1 (Fig S4F and Table S2). To investigate a possible regulation of major satellite transcripts by miR-30a-3p, miR-30d-3p and miR-30e-3p, we used miRNA inhibitors against the three miRNAs in WT mESCs. We transfected WT mESCs either with a negative control inhibitor or with a pool of miR-30a-3p, miR-30d-3p and miR-30e-3p inhibitors. We monitored the major satellite transcripts level 36 hours after transfection by RT-qPCR and identified an increase of around 2-fold upon transfection with the miR-30a-3p, miR-30d-3p and miR-30e-3p inhibitors compared to the negative control (Fig 4E). Similarly, transfecting WT mESCs with a miR-30-3p mimic significantly decreased major satellite transcript levels (Fig 4F). Taken together, these results indicate a role for the miR-30a-3p, miR-30d-3p and miR-30e-3p in fine-tuning major satellite transcript levels.

DISCUSSION

Since the discovery that AGO proteins can localize to the nucleus in mammalian cells, numerous studies have attempted to describe their nuclear functions (Meister, 2013). While in human cells, nuclear AGO's have been linked to functions in transcriptional gene regulation, splicing, chromatin organization and double-strand break repair (Janowski *et al*, 2006; Kim *et al*, 2006; Li *et al*, 2006; Hu *et al*, 2012; Cho *et al*, 2014; Portnoy *et al*, 2016; Huang *et al*, 2013; Alló *et al*, 2014; Shuaib *et al*, 2019; Ameyar-Zazoua *et al*, 2012; Agirre *et al*, 2015; Gao *et al*, 2014; Wang & Goldstein, 2016), little is known about their role during early embryonic development.

In this study, we aimed to assess a possible role for AGO1 in the distribution of constitutive heterochromatin in mESCs. AGO1 had previously been reported to interact with RNA Polymerase II in human cells, where AGO1 was linked to chromatin and active promoters (Huang *et al*, 2013; Alló *et al*, 2014; Shuaib *et al*, 2019). We therefore decided to conduct a genetic approach by depleting *Ago1* from WT mESCs (Fig S1A and B) and assessed by

immunofluorescence the localization of the repressive histone mark H3K9me3 and the heterochromatin protein HP1α in the mutant cell lines compared to WT mESCs (Fig 1). Surprisingly, we observed a redistribution of both H3K9me3 and HP1α away from pericentromeric regions in *Ago1*_KO mESCs (Fig 1). The redistribution of H3K9me3 and HP1α was found to be specific to the loss of AGO1, as reintroducing AGO1 could rescue the phenotype (Fig 2). We questioned whether major satellites residing within pericentromeric regions are upregulated at the transcript level in *Ago1*_KO mESCs. Indeed, we observed an increase of pericentromeric major satellite transcripts in *Ago1*_KO mESCs by RT-qPCR and RNA FISH, which could again be rescued by reintroducing AGO1 into *Ago1*_KO mESCs (Fig 3). This increase was not caused by a change in the number of chromocenters, as was confirmed by DNA FISH (Fig S3C and D). Finally, we wondered whether AGO1 could regulate pericentromeric transcripts by a miRNA-mediated mechanism and observed similar delocalization of both H3K9me3 and HP1α away from pericentromeric regions also in *Drosha*_KO mESCs, suggesting a role for miRNAs (Fig 4A and B). Using computational analysis, we identified that miR-30a-3p, miR-30d-3p and miR-30e-3p might target major satellite transcripts and that manipulating the amount of these miRNAs in WT mESCs using inhibitors or mimics inversely regulates major satellite transcript levels to some extent (Fig 4D, E, F). In addition, by analyzing the subcellular distribution of the AGO1, we found that a small fraction (10-15%) localized to the nucleus, leading us to the hypothesis that AGO1 loaded with miR-30-3p might directly regulate major satellite transcripts. Of note, the regulation observed here using mimics or inhibitors (Fig 4E and F) was lower (2-fold) than the one observed comparing WT and *Ago1*_KO mESCs (10-fold) (Fig 3B). We also observed an upregulation of HP1α at protein level in *Ago1*_KO (Fig S1F) and *Drosha*_KO mESCs (Fig S4A), leading us to propose that HP1α might also be directly regulated by miRNAs in mESCs (as also suggested by several miRNA binding sites in its 3'UTR and AGO2-Binding sites (Schäfer *et al*, 2021)). It would be interesting to further investigate this direct regulation of HP1α by miRNAs in a follow-up study.

An involvement of AGO proteins loaded with small RNAs in the regulation of pericentromeric regions has previously been reported in *S.pombe*, where Ago1 loaded with siRNAs is guided to pericentromeres (Verdel *et al*, 2004). Ago1 together with Tas3 and Chp1 forms the RNA-induced transcriptional silencing complex (RITS). The RITS is guided to centromeric repeats by siRNAs, which are derived from this region. Targeting the RITS complex to centromeric repeats is needed for the localization of the HP1α homolog Swi6 and the nucleation of heterochromatin H3K9me at these sites (Goto & Nakayama, 2012; Motamedi *et al*, 2004; Bühler *et al*, 2006; Verdel *et al*, 2004). However, our findings differ from the ones in yeast as we did not identify any small RNAs, derived from pericentromeric regions to be loaded in

AGO1. Though, there have been reports suggesting the presence of small RNAs from pericentromeric regions in mammalian cells (Hsieh *et al*, 2011; Kanellopoulou *et al*, 2005), we found that AGO1 in mESCs is probably guided to major satellite transcripts by specific miRNAs, miR-30a-3p, miR-30d-3p and miR-30e-3p.

Importantly, even though we identified a decrease of H3K9me3 at pericentromeric regions upon the depletion of *Ago1* in mESCs, this was accompanied by only a small impact on the global transcriptome and none regarding viability of *Ago1*_KO mESCs (Ngondo *et al*, 2018; Mueller *et al*, 2021). Ngondo et al., have reported that the depletion of *Ago1* does not affect the cell cycle nor their potential to differentiate (Ngondo *et al*, 2018; Van Stry *et al*, 2012). It appears that the loss of HP1α and H3K9me3 disturbs the environment more locally without affecting overall cell viability. While we do not currently know how mESCs cope with this loss, it is possible that the plasticity of stem cells or the reestablishment of heterochromatin at pericentromeric regions upon differentiation may be required for survival. As several studies in human and cancer cells have already described a nuclear role for the AGO proteins, especially also for AGO1 (Janowski *et al*, 2006; Kim *et al*, 2006; Li *et al*, 2006; Hu *et al*, 2012; Cho *et al*, 2014; Portnoy *et al*, 2016; Huang *et al*, 2013; Alló *et al*, 2014; Shuaib *et al*, 2019; Ameyar-Zazoua *et al*, 2012; Agirre *et al*, 2015), it will be interesting to study whether the decrease of H3K9me3 at pericentromeric regions also occurs in these cell types. Interestingly, the upregulation of major satellite transcripts in several cancer lines has already been described (Hall *et al*, 2012), however, we do not know whether this might be linked to a nuclear AGO1 function.

There are still open questions and further experiments required to identify the complete underlying molecular mechanism. How AGO1 regulates heterochromatin at pericentromeric regions and major satellite transcripts remains an open question. Our attempts to localize AGO1 at pericentromeric regions using IF or ChIP-qPCR approaches, using specific antibodies or AGO1-tagged cell lines, remained unsuccessful (data not shown). These negative results might come from the low amount of AGO1 in the nucleus (Fig 4C). New approaches or technical development are therefore required to precisely address AGO1 localization in the nucleus or chromatin in mESCs. Furthermore, in order to dissect a direct role of AGO1, it might be helpful in the future to assess whether AGO1 RNA binding activity is required for direct major satellite targeting *via* miRNAs.

In conclusion, our study reports a novel role for AGO1 in the nucleus of mESCs and we believe that these observations might help to motivate future research on the AGO proteins in early embryonic development.

MATERIALS AND METHODS

Mouse ESC lines

WT E14 (129/Ola background), *Ago1*_KO, AGO1 complemented *Ago1*_KO , and *Drosha*_KO (Cirera-Salinas *et al*, 2017) mESCs were cultured in Dulbecco's Modified Eagle Media (DMEM, Sigma-Aldrich), supplemented with 15% fetal bovine serum (FBS, Life Technologies), 100 U/ml LIF (Millipore), 0.1 mM 2-β-mercaptoethanol (Life Technologies), and 1% Penicillin/Streptomycin (Sigma-Aldrich). MESCs were cultured on 0.2% gelatin-coated culture flasks in the absence of feeder cells. The culture medium was changed daily and all cells were grown at 37°C in 8% CO_2.

CRISPR/Cas9 mediated gene knockout

The generation of the *Ago1*_KO1 cell line was previously published by (Ngondo *et al*, 2018). The *Ago1*_KO2 cell line was generated using a paired CRISPR/Cas9 approach, as described by (Wettstein *et al*, 2016). E14 mESCs were transfected with lipofectamine 2000 (Invitrogen) and the pX458-sgRNA_*Ago1*_5/6 (addgene #172470, #172471). After 48h, GFP-positive cells were single sorted into 96-well plates (TPP). In order to confirm the deletion, genotyping at DNA level was performed, with the primers PS_Ago1_FW/RW_1 listed in the Table S1. MESC clones were then amplified and the absence of AGO1 protein and RNA was additionally verified by Western blotting and RT-qPCR, respectively.

Generation of *Ago1*_KO complemented cell lines

For the rescue experiments, the AGO1 complemented *Ago1*_KO2 cells were obtained by stably transfecting the pMSCV_PIG_3xHA-AGO1 plasmid (addgene #170916) with lipofectamine 3000 (Invitrogen). Cells were grown for one week under puromycin selection and then sorted by FACS to select only GFP expressing cells. We sorted two mixed population into separate dishes of around 10000-20000 cells. The mixed populations were expanded and the expression of HA-AGO1 was tested by Western blot and Immunofluorescence (Fig 2A and S2A, B). For single clone generation, single cells expressing GFP were sorted into a 96-well plate and expanded. The expression of HA-AGO1 was tested by western blot (Fig S2C, D).

Cytoplasmic/ Nucleoplasmic/ Chromatin fractionation

Cytoplasmic/nucleoplasmic/chromatin fractionation was performed following the protocol of (Gagnon *et al*, 2014b). Cells were grown to near confluency in two 75 cm^2 (T75) flasks (TPP). 10 millions of WT mESCs were used. Freshly harvested cells were incubated for 10 min in ice-cold Hypotonic lysis buffer (HLB) complemented with EDTA-free protease inhibitor cocktail (Roche) and Phosphatase inhibitor cocktail (Roche). After centrifugation (800xg for 8 min at 4°C) the cytoplasmic fraction was transferred to a new tube containing 5M NaCl. Pellets were washed four times with HLB (200xg for 2 min). After the last wash ice-cold modified Wuarin-Schipler buffer (MWS) (10 mM Tris-HCl (pH 7.0), 4 mM EDTA, 0.3 M NaCl, 1 M urea, and 1% (vol/vol) IGEPAL-C630), complemented with EDTA-free protease inhibitor cocktail and Phosphatase inhibitor cocktail, was added and after vortexing, incubated for 15 min on ice. After centrifugation (1000xg for 5 min at 4°C) the nucleoplasmic fraction was transferred to a new tube. The chromatin pellet was washed twice with MWS buffer, vortexed, incubated on ice for 5 min and centrifuged at 500xg for 3 min at 4°C. Ice-cold NLB was added to the chromatin pellet, which was sonicated twice at 20% for 15 sec with 2 min incubations on ice in between. The three fractions were centrifuged for 15 min at 18000xg and the supernatant was transferred to a new tube.

The fractions were then analyzed by Western blot. To ensure proper representation of all the fractions, more of the nuclear (x4) and the chromatin (x8) fraction were loaded (Fig 4C).

Analysis of the Western blot signal was performed using ImageLab (Bio-Rad Laboratories). The intensity of the bands was calculated relative to the WT band. The intensities of the nuclear and chromatin fractions were adjusted according to the additional loading and the fact that they were resuspended in half the amount of buffer compared to the cytoplasm.

Western Blot Analysis

Total cellular proteins were extracted using RIPA lysing buffer (50 mM Tris-HCL pH 8.0, 150 mM NaCl, 1% IGEPAL CA-630, 0.5% sodium deoxycholate, 0.5% sodium dodecyl sulfate supplemented with EDTA-free protease inhibitor cocktail (Roche)). Protein concentration was determined by a Bradford assay (Bio-Rad Laboratories). Proteins were separated on an SDS-PAGE gel and transferred to a PVDF membrane (Sigma-Aldrich). Membranes were blocked for at least 30 min in blocking solution (5% milk in 1X TBS-T: TBS pH 7.6: 50 mM Tris-HCL, 150 mM NaCl and 0.1%

Tween-20) and incubated overnight with primary antibodies diluted in blocking solution at 4°C. Primary antibodies used were: HP1α (CST #2616, 1:2000), AGO1 (CST #5053, 1:2000), LAMIN B1 (abcam ab16048, 1:10000), TUBULIN (Sigma-Aldrich T6199, 1:10000), H3K9me3 (abcam ab8898, 1:2000), HA (Roche 3F10, 1:2000).

After washing 3 times in 1X TBS-T for 10 min, membranes were incubated with the secondary antibody for 1h at room temperature (rabbit-IgG HRP-linked 1:10000, Cell Signaling Technology (#7074), mouse-IgG HRP-linked 1:10000, Cell Signaling Technology (#7076), rat-IgG HRP-linked 1:10000 (#7077)). After incubation, membranes were washed again 3 times 10min in 1X TBS-T and developed using the Clarify Western ECL substrate kit (Bio-Rad) or SuperSignal West Femto (ThermoFisher Scientific). Membranes were imaged using the ChemiDoc MP imaging system (Bio-Rad Laboratories).

Analysis of the Western blot signal was performed using ImageLab (Bio-Rad Laboratories). Coomassie or TUBULIN was used as normalizer. Intensities of the bands were calculated relative to the WT band.

Immunofluorescence and analysis

Approximately 100000 cells were plated the night before into 6-well plates (TPP), containing coverslips coated with fibronectin (1:100 in 1X PBS, Merck). The next day, cells were washed once with 1X PBS.

For the H3K9me3 and HA staining, cells were fixed with ice-cold Methanol for 10 min at -20°C. After fixation they were washed 3 times with 1X PBS and blocked for 20 min in blocking solution (1% BSA in 1X PBS-Tween 20 (0.1%)).

For the HP1α staining, a nuclear pre-extraction was performed. Cells were washed once with ice-cold 1X PBS for 3 min on ice and then incubated in CSK buffer (0.1% Triton X-100, 10 mM PIPES, 100 mM NaCl, 3 mM $MgCl_2$, 300 mM Sucrose) for 3 min, also on ice. Afterwards cells were washed once with 1X PBS and fixed with 3.7% formaldehyde (Sigma-Aldrich) for 10 min at room temperature. After fixation, cells were washed twice with 1X PBS for 5 min at room temperature and then permeabilized with CSK buffer (same as above) for 4 min on ice. After two additional wash steps with 1X PBS at

room temperature, cells were blocked in blocking solution (1% BSA in 1X PBS-Tween 20 (0.1%)) for 20 min at room temperature.

After blocking, cells were incubated with the primary antibodies diluted in blocking solution (H3K9me3: ab8898, 1:500, HP1α: CST #2616, 1:200, HA: Roche 3F10, 1:250) for 1h at room temperature. Coverslips were washed three times for 5 min at room temperature with 1X PBS-Tween 20 (0.1%). Then, cells were incubated with secondary antibodies diluted in blocking solution (1:2000, Invitrogen) for 1 h at room temperature in the dark. Again, coverslips were washed three times for 5 min at room temperature with 1X PBS-Tween 20 (0.1%) and once with 1X PBS. Counterstain with DAPI (0.1 µl/ml) in 1X PBS was performed for 4 min at room temperature. Cells were washed once with 1X PBS and mounted on microscopy slides on a drop of antifade medium (Vectashield, Vector Laboratories). Slides were imaged on a DeltaVision Multiplexed system with an Olympus IX71 inverse microscope equipped with a 60x 1.4NA DIC Oil PlanApoN objective and a pco.edge 5.5 camera, provided by the ScopeM facility of ETH.

For image analysis, deconvolved images were processed with Fiji (Schindelin *et al*, 2012). A Z-projection of the Max intensity has been performed for each image and used for further analysis. Foci count and intensity analysis was performed on the Z-projected images, with the help of CellProfiler (Mcquin *et al*, 2018). In CellProfiler, nuclei were identified by using the IdentifyPrimaryObjects module and the Otsu thresholding method. Nuclei were edited manually and the DAPI and H3K9me3 was enhanced with the EnhanceOrSupressFeatures module to detect speckles. Foci were identified by using IdentifyPrimaryObject. For the DAPI foci, the RobustBackground was used as a thresholding method and the threshold strategy was set to Global. Typical diameter of objects, in pixel units was set to 5-35. For the H3K9me3 foci the same thresholding method and strategy was used, but the typical diameter of objects, in pixel units was set to 7-35. Foci were related to the edited nuclei and the H3K9me3 foci were related to the DAPI foci. The MeasureObjectIntensity module was used to measure object intensity and foci count and results were exported to a csv file. Overlayed objects were saved as png.

RNA extraction and quantitative RT-qPCR Analysis

RNA extraction and RT PCR analysis has been performed as previously described by (Bodak & Ciaudo, 2016). Briefly, total RNA from mESC pellets was extracted using Trizol (Life Technologies) according to standard protocols. RNA quality was checked, by running 1 µg on a 1% agarose gel (Sigma).

For qPCR on major satellite transcripts, 20 µg of RNA was treated twice with 1U of DNaseI (Qiagen) per µg of RNA. RiboLock was added to reduce RNA degradation. DNase treated RNA was purified using Direct-zol RNA mini prep kit (Zymo Research). Reverse transcription and qPCR were performed as described above.

Primers are listed in the supplementary Table S1.

RNA FISH

The plasmid pCR4 Maj9-2 (a kind gift from the Almouzni lab, originally from (Lehnertz *et al*, 2003)) was used to generate the RNA FISH probe by nick translation (Abott). In brief, 2 µg of plasmid, 3 µl of nick translation enzyme, 2.5 µl 0.2 mM red-dUTP, 5 µl 0.1 mM dTTP, 10 µl 0.1 mM dNTP mix and 5 µl 10X nick translation buffer were incubated for 15 h at 15°C. Nick translation efficiency was checked for by running 3 µl probe on a 1% agarose gel (Sigma). The rest of the probe was cleaned-up with the Zymoclean Gel DNA Recovery Kit (Zymo Research). The probe was dried down to 5 µl using a speed vac and then resuspended in hybridization solution (50 µl Deionized Formamide, 10 µl 20X SSC, 2 µl 100mg/ml BSA, 20 µl 50% Dextran Sulfate, 3 µl Salmon Sperm, 10 µl RVC). Prior to use, the probe was diluted 1:2 in hybridization solution.

Approximately 150000 cells were plated the night before into 6-well plates, containing coverslips coated with fibronectin (1:100 in 1X PBS, Merck). A nuclear pre-extraction was performed. Cells were washed once with ice-cold 1X PBS for 3 min on ice and then incubated in CSK buffer (0.1% Triton X-100, 10 mM PIPES, 100 mM NaCl, 3 mM $MgCl_2$, 300 mM Sucrose) for 3 min, also on ice. Afterwards cells were washed once with 1X PBS and fixed with 3.7% formaldehyde (Sigma-Aldrich) for 10 min at room temperature. After fixation, cells were washed twice with 1X PBS for 5 min at room temperature and then permeabilized with CSK buffer (same as above) for 4 min on ice. After two additional wash steps with 1X PBS at room temperature, cells were blocked in blocking solution (1% BSA in 1X PBS and RVC (1 mM)) for 30 min at room temperature. Then coverslips were washed once with 2X SSC

and dehydrated with ethanol (70% EtOH for 3 min, 90% EtOH for 3 min, 100% EtOH for 3 min). The probe was denatured for 5 min at 76°C. 10µl of the denatured probe (diluted 1:2 in hybridization buffer) was spotted on a baked slide. The coverslips were air-dried and placed on the spotted probe. The coverslips were sealed with rubber cement and then incubated overnight at 37°C in a humid chamber. The next day, coverslips were washed twice with 50% Formamide/2X SSC for 5 min at 37°C and then once for 5 min with 2X SSC at room temperature. Counterstain with DAPI (0.1 µl/ml) in 2X SSC was performed for 4 min at room temperature. Coverslips were washed again once in 2xSSC and once 1X PBS and then mounted on microscopy slides on a drop of antifade medium (Vectashield, Vector Laboratories). Slides were image on a DeltaVision Multiplexed system provided by the ScopeM facility of ETH as above.

For image analysis, deconvolved images were processed with Fiji (Schindelin *et al*, 2012). A Z-projection of the Max intensity has been performed for each image and used for further analysis. RNA Foci were counted by eye. All Z-projected images of one replicate were opened using the Fiji software and were set to the same intensity.

DNA FISH

DNA FISH was performed exactly as described for the RNA FISH. The only differences, are that no RVC was used in the blocking solution and the samples were denatured by incubating the slides at 76°C for 5 min once the coverslips were placed on the spotted probe and sealed with rubber cement.

ChIP and ChIP-qPCR analysis

Four million cells were plated the night before into a gelatin-coated 60.1 cm^2 (B10) dish (TPP). For each condition, two B10 dishes were prepared in parallel. Cells were crosslinked with 1% formaldehyde in DMEM for 10 min at room temperature. The reaction was quenched with glycine (125 mM, PanReac Applichem) for 5 min at room temperature. Cells were washed once with ice-cold 1X PBS and then swelling buffer (5 mM HEPES pH 8, 85 mM KCl, 0.5% IGEPAL-CA630, protease inhibitor cocktail (Roche)) was added to the cells. Cells were scraped and transferred to a 15 ml falcon (Greiner), where they were incubated for 15 min on ice. Cells were centrifuged 5 min at 2000

rpm at 4°C, to pellet the nuclei. Afterwards, nuclei were washed again with swelling buffer followed by another centrifugation (250 g at 4°C for 5 min). The nuclei pellet was lysed in 400 µl RIPA buffer 1% SDS (1X PBS, 1% IGEPAL-C630, 0.5% sodium deoxycholate, 1% sodium dodecyl sulfate, protease inhibitor cocktail (Roche)) and incubated on ice for 10 min. The lysates were sonicated on a Bioruptor (Diagenode) for 30 min, 30s on and 30s off cycles at 4°C. Lysates were centrifuged at max speed for 15 min at 4°C. The supernatant was retrieved into a new 2 ml Eppendorf tube and diluted 10 times with RIPA buffer 0% SDS (1X PBS, 1% IGEPAL-C630, 0.5% sodium deoxycholate, protease inhibitor cocktail (Roche)) to obtain a concentration of 0.1% sodium dodecyl sulfate. 10% of chromatin was taken away for Input calculation, the rest of the chromatin was snap-frozen and stored at -80°C. Input DNA was treated with 10 µg RNase A for 1 h at 37°C followed by a proteinase K treatment (40 µg) for 1-2 h. DNA was extracted with phenol/chloroform (Sigma-Aldrich) and concentration was measured and used to calculate the total amount of chromatin in each sample.

For the pulldown, 20 µg of chromatin was precleared with 10 µl of Dynabeads protein G (ThermoFisher Scientific), previously washed three times with RIPA 0.1% SDS (1X PBS, 1% IGEPAL-C630, 0.5% sodium deoxycholate, 0.1% sodium dodecyl sulfate, protease inhibitor cocktail (Roche)), for 2 h on the wheel at 4°C. 1/10 of the pre-cleared chromatin was taken away and stored temporarily at -20°C, this was later used as the Input. The rest of the pre-cleared chromatin was transferred into a new 1.5 ml Eppendorf tube and incubated with 2 µg of antibody for each condition overnight at 4°C (H3K9me3: ab8898, rabbit-IgG: NI01). 10 µl of Dynabeads protein G (ThermoFisher Scientific) was added to the chromatin-antibody complexes and incubated 4 h on the wheel at 4°C. Samples were placed on the magnetic rack and the supernatant was discarded. Samples were washed twice with wash buffer 1 (16.7 mM Tris-HCL pH 8, 0.167 M NaCl, 0.1% SDS, 1% Triton X-100) for 5 min rotating at room temperature. Then they were washed once with wash buffer 2 (16.7 mM Tris-HCl pH 8, 0.5M NaCl, 0.1% SDS, 1% Triton X-100) for 5 min rotating at room temperature and twice in LiCl wash buffer (0.25 M LiCl, 0.5% sodium deoxycholate, 1 mM EDTA pH 8, 10 mM Tris-HCl pH 8, 0.5% IGEPAL-CA630) for 5 min rotating at room temperature. Finally, the samples were washed twice in TE buffer (10 mM Tris-HCl pH 8, 5 mM EDTA pH 8) for 5 min rotating at room temperature. Samples were incubated in 300 µl elution buffer (1% SDS, 100 mM $NaHCO_3$) for 30 min at 37°C shaking at 900 rpm. Samples were placed on a magnetic rack and the supernatant transferred into a new Eppendorf tube containing 38.5 µl Proteinase K mix (15 µl 1M Tris-HCl pH 8, 15 µl 5M NaCl, 7.5 µl 0.5M EDTA

pH 8, 1 µl Proteinase K (20 mg/ml)). Also 300 µl elution buffer and 38.5 µl Proteinase K mix was added to the Inputs. Pull-downs and Inputs were incubated at 50°C for 3 h shaking at 1100 rpm and then at 65°C overnight. DNA was treated with 10 µg of RNase A for 45 min at 37°C and extracted with a phenol/chloroform extraction, followed by an ethanol precipitation.

ChIPed and Input DNA was diluted 1:10 prior to the qPCR for the control Primers (Dazl, MusD and the intergenic region) and 1:50 prior to the qPCR for the major satellites. The qPCR was performed with the KAPA SYBR Fast qPCR Kit (Kapa Biosystems) and analyzed on a LightCycler 480 (Roche). The enrichment was calculated with the $2^{-\Delta\Delta CT}$ method over input. Control regions (Dazl, MusD (Karimi *et al*, 2011)) were represented as enrichment over the intergenic region (Ngondo *et al*, 2018). The enrichment for the major satellites was represented as the enrichment compared to WT. Primers are listed in Table S1.

Major satellite computational analysis and binding site identification

RepeatMasker annotations were obtained from UCSC for the mm10 mouse reference genome **(**http://hgdownload.soe.ucsc.edu/goldenPath/mm10/database/rmskOutCurrent.txt.gz) and filtered for major satellites (GSAT_MM) (Bao *et al*, 2015; Smit *et al*, 2013). Most regions annotated as major satellites were rather short (< 1000 bps) and we only considered 4 regions, where the genome sequence contained > 20 Kbps long major satellite regions. One of them was mapped into the X-chromosome and another one to chromosome 9. The other two fell into genomic contigs that could not be assigned to any chromosome (JH584304.1 and GL456383.1). For these four annotated regions, 8mer binding sites were scanned and counted for each mESC-expressed miRNA (Table S2). Small RNA-seq from WT mESCs has been previously analyzed in (Schäfer *et al*, 2021) and RIP-small RNA-seq in (Ngondo *et al*, 2018).

miRNA inhibitor and mimic transfection

Approximately 300 000 - 400 000 WT mESCs were plated the night before into a gelatin-coated 60.1 cm^2 (B10) dish (TPP). The next day, for the miRNA inhibitor transfection, WT mESCs were either transfected with RNAiMax (Invitrogen) and 30 nM of a negative control inhibitor (Ambion, #4464074) or with RNAiMax (Invitrogen) and a mix of miR-30a-3p, miR-30d-3p and miR-30e-3p inhibitors, 10 nM

for each inhibitor (Ambion, #4464084). For the miRNA mimic transfection, WT mESCs were either transfected with RNAiMax (Invitrogen) and 30 nM of a negative control mimic (Dharmacon, CN-001000-01-05) or with RNAiMax (Invitrogen) and 30 nM of miR-30e-3p mimics (Dharmacon, C-310467-07-0002). 36 h later, the cell pellet was collected. Briefly, cells were washed once with 1X PBS (Life Technologies), then trypsinized with 0.05% Trypsin-EDTA (Life Technologies) for 5 min at 37°C. Trypsinization was stopped, by adding medium and spinning the cells down for 5 min at 182xg. The cell pellet was washed once in 1X PBS (Life Technologies), spun down 5 min at 182xg and then stored at -80°C.

QUANTIFICATION AND STATISTICAL ANALYSIS

See Methods Details for details on quantification and statistical analysis. In general, statistical analysis was performed using PRIMS 8 as indicated in the figure legends.

DATA AVAILABILITY

Small RNA-seq (Schäfer *et al*, 2021) and RIP-small RNA-seq (Ngondo *et al*, 2018) used in this study have been deposited in the GEO repository, analyzed results are provided in Table S2.

Reviewer access:

- GSE110945 token wvebgccuhrabhqf (Small RNA profiling of WT E14 mESCs)
- GSE80211 open (RIP-small RNA seq)

Acknowledgments

We would like to thank the members of the Ciaudo Lab, Dr. Tobias Beyer and Prof. Madhav Jagannathan (ETH) for fruitful discussions and the critical reading of this manuscript. We would also like to thank the Santoro lab for help with the ChIP protocol. This work was supported by the Swiss National Science Foundation (grants 31003A_173120 and 310030_196861) to C.C, R.A and M.M were supported by the NCCR RNA and disease. We are also thankful to the Scientific Centre for Optical and Electron Microscopy (ScopeM, ETH Zurich) for their support for imaging and the Flow Cytometry Core Facility of ETH for their help with FACS.

Author Contributions

Conceptualization, MM, TF and CC.; laboratory experiments, MM, TF, JL, PS, RA, PN, VH; computational analysis, MS.; writing—original draft preparation, MM, TF and CC.; writing—review and editing, CC.; expertise and editing, PN.; visualization, MM, TF, MS and CC.; supervision, CC; funding acquisition, CC. All authors have read and agreed to the published version of the manuscript.

Conflict of Interests

The authors declare no financial and non-financial competing interests.

Supporting Information

Supplemental Figures

Table S1

Table S2

References

Agirre E, Bellora N, Alló M, Pagès A, Bertucci P, Kornblihtt AR & Eyras E (2015) A chromatin code for alternative splicing involving a putative association between CTCF and HP1aα proteins. *BMC Biol* 13

Akhtar A & Gasser SM (2007) The nuclear envelope and transcriptional control. *Nat Rev Genet* 8: 507–517

Alisch RS, Jin P, Epstein M, Caspary T & Warren ST (2007) Argonaute2 is essential for mammalian gastrulation and proper mesoderm formation. *PLoS Genet* 3: 2565–2571

Alló M, Agirreb E, Bessonovc S, Bertucci P, Acuña LG, Buggiano V, Bellorab N, Singhb B, Petrillo E, Blaustein M, *et al* (2014) Argonaute-1 binds transcriptional enhancers and controls constitutive and alternative splicing in human cells. *Proc Natl Acad Sci U S A* 111: 15622–15629

Ameyar-Zazoua M, Rachez C, Souidi M, Robin P, Fritsch L, Young R, Morozova N, Fenouil R, Descostes N, Andrau J-C, *et al* (2012) Argonaute proteins couple chromatin silencing to alternative splicing. *Nat Struct Mol Biol*

Bannister AJ, Zegerman P, Partridge JF, Miska EA, Thomas JO, Allshire RC & Kouzarides T (2001) Selective recognition of methylated lysine 9 on histone H3 by the HP1 chromo domain. *Nature* 410: 120–124

Bao W, Kojima KK & Kohany O (2015) Repbase Update, a database of repetitive elements in eukaryotic genomes. *Mob DNA* 6: 4–9

Bartel DP (2018) Metazoan MicroRNAs. *Cell* 173: 20–51

Bernard P, Maure JF, Partridge JF, Genier S, Javerzat JP & Allshire RC (2001) Requirement of heterochromatin for cohesion at centromeres. *Science (80-)* 294: 2539–2542

Bodak M & Ciaudo C (2016) Monitoring Long Interspersed Nuclear Element 1 Expression During Mouse Embryonic Stem Cell Differentiation. *Transposons and Retrotransposons* 1400

Bodak M, Cirera-Salinas D, Luitz J & Ciaudo C (2017) The role of RNA interference in stem cell biology: Beyond the mutant phenotypes. *JMB* 429: 1532–1543

Boroviak T, Stirparo GG, Dietmann S, Hernando-Herraez I, Mohammed H, Reik W, Smith A, Sasaki E, Nichols J & Bertone P (2018) Single cell transcriptome analysis of human, marmoset and mouse embryos reveals common and divergent features of preimplantation development. *Development* 145

Bühler M, Verdel A & Moazed D (2006) Tethering RITS to a nascent transcript initiates RNAi- and heterochromatin-dependent gene silencing. *Cell* 125: 873–86

Cheloufi S, Dos Santos CO, Chong MMW, Hannon GJ & Cheloufi et al. 2010 (2010) A dicer-independent miRNA biogenesis pathway that requires Ago catalysis. *Nature* 465: 584–9

Cho S, Park JS & Kang YK (2014) AGO2 and SETDB1 cooperate in promoter-targeted transcriptional silencing of the androgen receptor gene. *Nucleic Acids Res* 42: 13545–13556

Cirera-Salinas D, Yu J, Bodak M, Ngondo RP, Herbert KM & Ciaudo C (2017) Noncanonical function of DGCR8 controls mESC exit from pluripotency. *J Cell Biol* 216: 355–366

DeVeale B, Swindlehurst-Chan J & Blelloch R (2021) The roles of microRNAs in mouse development. *Nat Rev Genet*

Fallatah B, Shuaib M, Adroub S, Paytuví-Gallart A, Della Valle F, Nadeef S, Lanzuolo C & Orlando V (2021) Ago1 controls myogenic differentiation by regulating eRNA-mediated CBP-guided epigenome reprogramming. *Cell Rep* 37

Gagnon KT, Li L, Chu Y, Janowski BA & Corey DR (2014a) RNAi factors are present and active in human cell nuclei. *Cell Rep* 6: 211–221

Gagnon KT, Li L, Janowski BA & Corey DR (2014b) Analysis of nuclear RNA interference in human cells by subcellular fractionation and Argonaute loading. *Nat Protoc* 9: 2045–2060

Gao M, Wei W, Li MM, Wu YS, Ba Z, Jin KX, Li MM, Liao YQ, Adhikari S, Chong Z, *et al* (2014) Ago2 facilitates Rad51 recruitment and DNA double-strand break repair by homologous recombination. *Cell Res* 24: 532–541

Goto DB & Nakayama J (2012) RNA and epigenetic silencing: Insight from fission yeast. *Dev Growth Differ* 54: 129–141

Guenatri M, Bailly D, Maison C & Almouzni G (2004) Mouse centric and pericentric satellite repeats form distinct functional heterochromatin. *J Cell Biol* 166: 493–505

Hall LE, Mitchell SE & O'Neill RJ (2012) Pericentric and centromeric transcription: A perfect balance required. *Chromosom Res* 20: 535–546

Houlard M, Berlivet S, Probst A V., Quivy JP, Héry P, Almouzni G & Gérard M (2006) CAF-1 is essential for heterochromatin organization in pluripotent embryonic cells. *PLoS Genet* 2: 1686–1696

Hsieh CL, Lin CL, Liu H, Chang YJ, Shih CJ, Zhong CZ, Lee SC & Tan BCM (2011) WDHD1 modulates the post-transcriptional step of the centromeric silencing pathway. *Nucleic Acids Res* 39: 4048–4062

Hu J, Chen Z, Xia D, Wu J, Xu H & Ye ZQ (2012) Promoter-associated small double-stranded RNA interacts with heterogeneous nuclear ribonucleoprotein A2/B1 to induce transcriptional activation. *Biochem J* 447: 407–416

Huang V, Zheng J, Qi Z, Wang J, Place RF, Yu J, Li H & Li L-C (2013) Ago1 Interacts with RNA Polymerase II and Binds to the Promoters of Actively Transcribed Genes in Human Cancer Cells. *PLoS Genet* 9: e1003821

Hyun K, Jeon J, Park K & Kim J (2017) Writing, erasing and reading histone lysine methylations. *Exp Mol Med* 49

Janowski B a, Huffman KE, Schwartz JC, Ram R, Nordsell R, Shames DS, Minna JD & Corey DR (2006) Involvement of AGO1 and AGO2 in mammalian transcriptional silencing. *Nat Struct Mol Biol* 13: 787–92

Kanellopoulou C, Muljo S a, Kung AL, Ganesan S, Drapkin R, Jenuwein T, Livingston DM & Rajewsky K (2005) Dicer-deficient mouse embryonic stem cells are defective in differentiation and centromeric silencing. *Genes Dev* 19: 489–501

Karimi MM, Goyal P, Maksakova I a, Bilenky M, Leung D, Tang JX, Shinkai Y, Mager DL, Jones S, Hirst M, *et al* (2011) DNA methylation and SETDB1/H3K9me3 regulate predominantly distinct sets of genes, retroelements, and chimeric transcripts in mESCs. *Cell Stem Cell* 8: 676–87

Kelly TJ, Brümmer A, Hooshdaran N, Tariveranmoshabad M & Zamudio JR (2019) Temporal Control of the TGF-β Signaling Network by Mouse ESC MicroRNA Targets of Different Affinities. *Cell Rep* 29: 2702-2717.e7

Kim DH, Villeneuve LM, Morris K V & Rossi JJ (2006) Argonaute-1 directs siRNA-mediated transcriptional gene silencing in human cells. *Nat Struct Mol Biol* 13: 793–7

Komissarov AS, Gavrilova E V., Demin SJ, Ishov AM & Podgornaya OI (2011) Tandemly repeated DNA families in the mouse genome. *BMC Genomics* 12

Lachner M, O'Carroll D, Rea S, Mechtler K & Jenuwein T (2001) Methylation of histone H3 lysine 9 creates a binding site for HP1 proteins. *Nature* 410: 120–124

Lehnertz B, Ueda Y, Derijck AAHAA, Braunschweig U, Perez-Burgos L, Kubicek S, Chen T, Li E, Jenuwein T & Peters AHFMH (2003) Suv39h-mediated histone H3 lysine 9 methylation directs DNA methylation to major satellite repeats at pericentric heterochromatin. *Curr Biol* 13: 1192–1200

Li LCC, Okino STT, Zhao H, Pookot D, Place RFF, Urakami S, Enokida H & Dahiya R (2006) Small dsRNAs induce transcriptional activation in human cells. *PNAS* 103: 17337–17342

Li X, Wang X, Cheng Z & Zhu Q (2020) AGO2 and its partners: a silencing complex, a chromatin modulator, and new features. *Crit Rev Biochem Mol Biol* 0: 1–21

Liu J, Carmell MAA, Rivas FV V, Marsden CGG, Thomson JMM, Song J-JJ, Hammond SMM, Joshua-Tor L & Hannon GJJ (2004) Argonaute2 is the catalytic engine of mammalian RNAi. *Science (80-)* 305: 1437–1441

Lykke-Andersen K, Gilchrist MJ, B. GJ, Partha D, Eric M & Magdalena Z-G (2008) Maternal Argonaute 2 Is Essential for Early Mouse Development at the Maternal-Zygotic Transition. *Mol Biol Cell* 19: 4383–4392

Mcquin C, Goodman A, Chernyshev V, Kamentsky L, Cimini A, Karhohs KW, Doan M, Ding L, Rafelski SM, Thirstrup D, *et al* (2018) Cellprofiler 3.0: Next-generation image processing for biology. *PLoS Biol* 16: 1–17

Meister G (2013) Argonaute proteins: functional insights and emerging roles. *Nat Rev Genet* 14: 447–59

Modzelewski AJ, Holmes RJ, Hilz S, Grimson A & Cohen PE (2012) AGO4 Regulates Entry into Meiosis and Influences Silencing of Sex Chromosomes in the Male Mouse Germline. *Dev Cell* 23: 251–264

Morita S, Horii T, Kimura M, Goto Y, Ochiya T & Hatada I (2007) One Argonaute family member, Eif2c2 (Ago2), is essential for development and appears not to be involved in DNA methylation. *Genomics* 89: 687–696

Motamedi MRR, Verdel A, Colmenares SUU, Gerber SAA, Gygi SPP & Moazed D (2004) Two RNAi complexes, RITS and RDRC, physically interact and localize to noncoding centromeric RNAs. *Cell* 119: 789–802

Mueller M, Schaefer M, Faeh T, Spies D, Peña-Hernández R, Santoro R & Ciaudo C (2021) ARGONAUTE proteins regulate a specific network of genes through KLF4 in mouse embryonic stem cells. *bioRxiv*: 2021.10.18.464771

Müller M, Fazi F & Ciaudo C (2020) Argonaute Proteins□: From Structure to Function in Development and Pathological Cell Fate Determination. *Front Cell Dev Biol* 7: 1–10

Ngondo RP, Cirera-Salinas D, Yu J, Wischnewski H, Bodak M, Vandormael-Pournin S,

Geiselmann A, Wettstein R, Luitz J, Cohen-Tannoudji M, *et al* (2018) Argonaute 2 Is Required for Extra-embryonic Endoderm Differentiation of Mouse Embryonic Stem Cells. *Stem Cell Reports* 10: 1–16

Nishi K, Nishi A, Nagasawa T & Ui-Tei K (2013) Human TNRC6A is an Argonaute-navigator protein for microRNA-mediated gene silencing in the nucleus. *RNA* 19: 17–35

Nonaka N, Kitajima T, Yokobayashi S, Xiao G, Yamamoto M, Grewal SIS & Watanabe Y (2002) Recruitment of cohesin to heterochromatic regions by Swi6/HP1 in fission yeast. *Nat Cell Biol* 4: 89–93

Portnoy V, Lin SHS, Li KH, Burlingame A, Hu ZH, Li H & Li LC (2016) SaRNA-guided Ago2 targets the RITA complex to promoters to stimulate transcription. *Cell Res* 26: 320–335

Probst A V. & Almouzni G (2008) Pericentric heterochromatin: Dynamic organization during early development in mammals. *Differentiation* 76: 15–23

Probst A V, Dunleavy E & Almouzni G (2009) Epigenetic inheritance during the cell cycle. *Nat Rev Mol Cell Biol* 10: 192–206

Probst A V, Okamoto I, Casanova M, Marjou F El & Baccon P Le (2010) A Strand-Specific Burst in Transcription of Pericentric Satellites Is Required for Chromocenter Formation and Early Mouse Development. *Dev Cell* 19: 625–638

Rudert F, Bronner S, Garnier JW & Dollé P (1995) Transcripts from opposite strands of γ satellite DNA are differentially expressed during mouse development. *Mamm Genome* 6: 76–83

Sarshad AA, Juan AH, Muler AIC, Anastasakis DG, Wang X, Genzor P, Feng X, Tsai P-F, Sun H-W, Haase AD, *et al* (2018) Argonaute-miRNA Complexes Silence Target mRNAs in the Nucleus of Mammalian Stem Cells. *Mol Cell* 71: 1040-1050.e8

Schäfer M, Nabih A, Spies D, Bodak M, Stalder P, Ngondo RP, Liechti LA, Sajic T, Aebersold R, Gatfield D, *et al* (2021) Integrative analysis allows a global and precise identification of functional miRNA target genes in mESCs. *bioRxiv*

Schindelin J, Arganda-Carreras I, Frise E, Kaynig V, Longair M, Pietzsch T, Preibisch S, Rueden C, Saalfeld S, Schmid B, *et al* (2012) Fiji: An open-source platform for biological-image analysis. *Nat Methods* 9: 676–682

Shivram H, Le S V. & Iyer VR (2019) MicroRNAs reinforce repression of PRC2 transcriptional targets independently and through a feed-forward regulatory network. *Genome Res* 29: 184–192

Shuaib M, Parsi KM, Thimma M, Ravasi T, Carninci P, Orlando V, Shuaib M, Parsi KM, Thimma M, Adroub SA, *et al* (2019) Nuclear AGO1 Regulates Gene Expression by Affecting Chromatin Architecture in Human Cells. *Cell Syst* 9: 446-458.e6

Smit A, Hublex R & Green P RepeatMasker Open-4.0. [PREPRINT]

Smit A, Hubley R & Green P (2013) RepeatMasker Open-4.0. (www.repeatmasker.org)

Solovei I, Kreysing M, Lanctôt C, Kösem S, Peichl L, Cremer T, Guck J & Joffe B (2009) Nuclear Architecture of Rod Photoreceptor Cells Adapts to Vision in Mammalian Evolution. *Cell* 137: 356–368

Storer J, Hubley R, Rosen J, Wheeler TJ & Smit AF (2021) The Dfam community resource of transposable element families, sequence models, and genome annotations. *Mob DNA* 12: 1–14

Van Stry M, Oguin TH, Cheloufi S, Vogel P, Watanabe M, Pillai MR, Dash P, Thomas PG, Hannon GJ & Bix M (2012) Enhanced Susceptibility of Ago1/3 Double-Null Mice to Influenza A Virus Infection. *J Virol* 86: 4151–7

Verdel A, Jia S, Gerber S, Sugiyama T, Gygi S, Grewal SIS & Moazed D (2004) RNAi-Mediated Targeting of Heterochromatin by the RITS. *Science (80-)* 303: 672–676

Vissel B & Choo KH (1989) Mouse major (γ) satellite DNA is highly conserved and organized into extremely long tandem arrays: Implications for recombination between nonhomologous chromosomes. *Genomics* 5: 407–414

Wang Q & Goldstein M (2016) Small RNAs recruit chromatin-modifying enzymes MMSET and Tip60 to reconfigure damaged DNA upon double-strand break and facilitate repair. *Cancer Res* 76: 1904–1915

Wettstein R, Bodak M & Ciaudo C (2016) Generation of a Knockout Mouse Embryonic Stem Cell Line Using a Paired CRISPR/Cas9 Genome Engineering Tool. *Methods Mol Biol* 1341: 321–43

Figure & Figure Legends

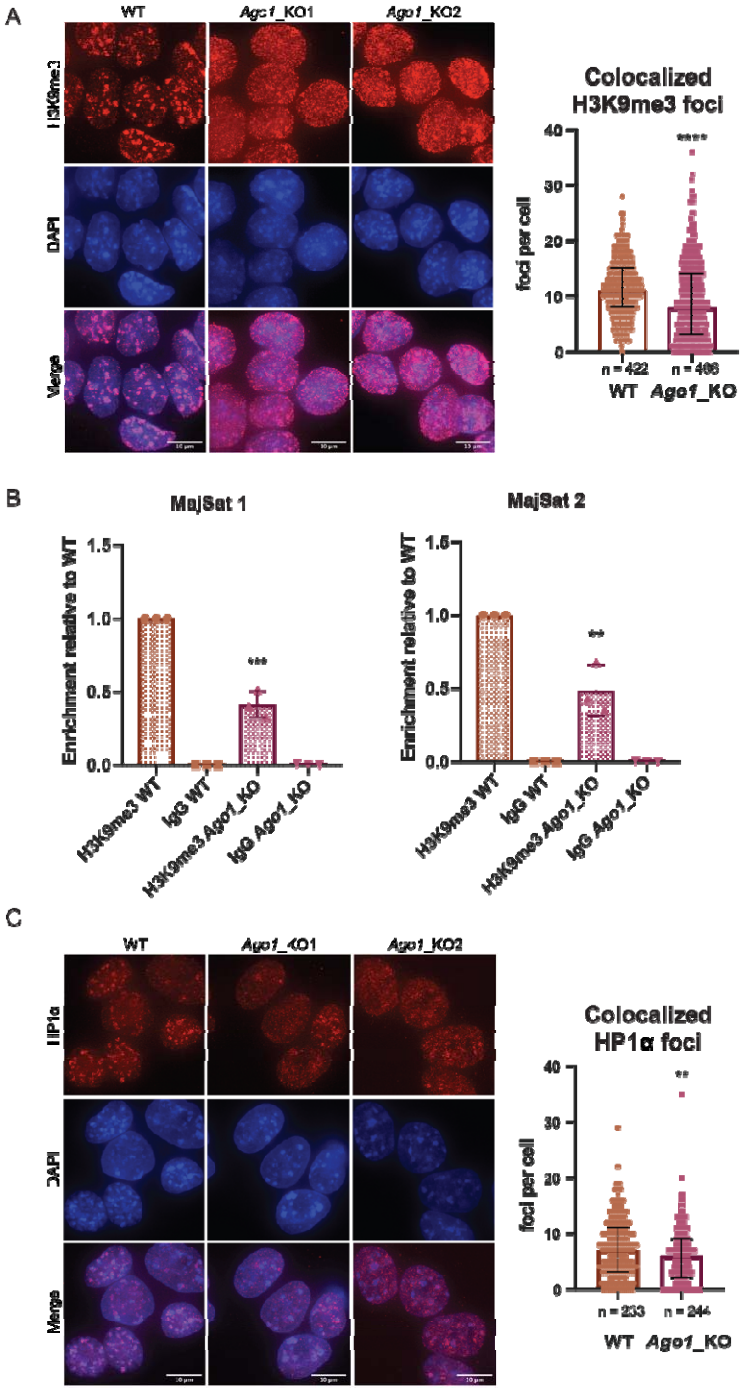

Figure 1. Distribution of H3K9me3 and HP1α at pericentromeric regions in WT versus *Ago1*_KO mESCs.

(A) Left: Representative IF images of H3K9me3 in WT and *Ago1*_KO mESCs. scale bar = 10 μm. Right: Quantification of foci counts for H3K9me3 that colocalizes with DAPI regions in WT and *Ago1*_KO mESCs. Due to the bimodal distribution of H3K9me3 foci in *Ago1*_KO mESCs, the graph

shows the median distribution with the interquartile range. **** = p value < 0.0001, Mann-Whitney test for n=3 independent experiments.

(B) ChIP-qPCR in WT and *Ago1*_KO mESCs. Pulldowns were performed with an antibody against H3K9me3 and a control IgG antibody. qPCR has been performed on major satellite primer set 1 and 2 (Table S1). The enrichment was calculated over input and represented relative to the WT H3K9me3 pulldown. *** = p value < 0.001 and ** = p value < 0.01, unpaired t-test for n=3 independent experiments. The *Ago1*_KO1 and *Ago1*_KO2 have been combined in this experiment. IgG error bars clipped at axis limit.

(C) Left: Representative IF images of HP1α in WT and *Ago1*_KO mESCs. scale bar = 10 μm. Right: Quantification of foci count for HP1α that colocalizes with DAPI regions in WT and *Ago1*_KO mESCs. The graph shows the median distribution with the interquartile range. ** = p value < 0.01, Mann-Whitney test for n=3 independent experiments. For the quantification *Ago1*_KO1 and *Ago1*_KO2 were combined.

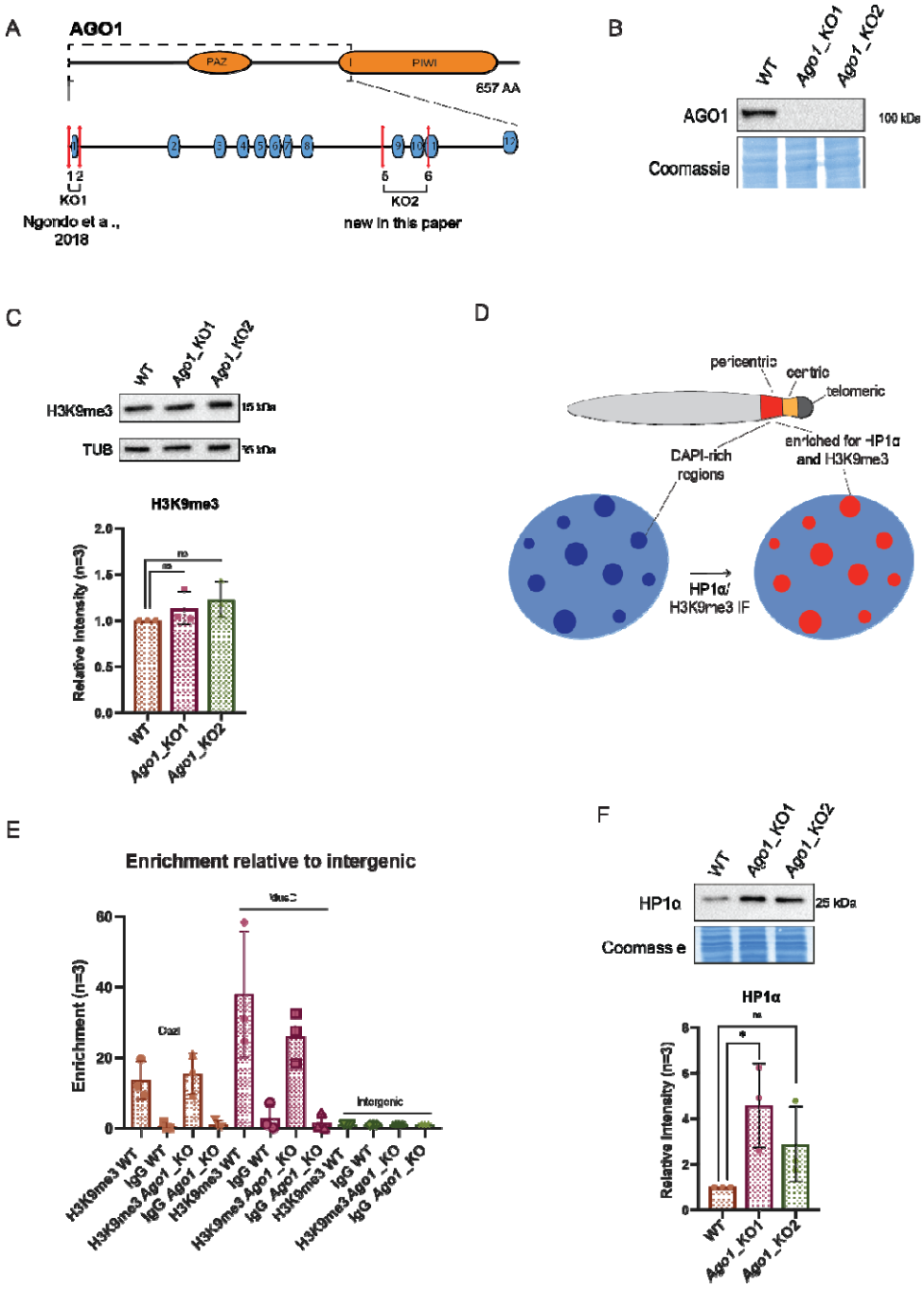

Figure S1. Assessment of pericentromeric factors in WT versus *Ago1*_KO mESCs.

(A) Schematic representation of the *Ago1*_KO paired CRISPR/Cas9 approach. Numbers 1, 2 and 5, 6 represent sgRNAs used to generate the KO lines. *Ago1*_KO1 has already been published by (Ngondo *et al*, 2018).

(B) Representative Western blots for AGO1 in WT, *Ago1*_KO1 and *Ago1*_KO2 mESCs out of n=3 independent experiments.

C) Representative Western blots for H3K9me3 in WT, *Ago1*_KO1 and *Ago1*_KO2 mESCs and quantification. ns = non-significant, unpaired t-test for n=3 independent experiments.

(D) Schematic representation of mouse pericentromeric regions. Shown are the DAPI-rich regions that are enriched for HP1α and H3K9me3 and visualized by IF.

(E) ChIP-qPCR in WT and *Ago1*_KO mESCs. Pulldowns were performed with an antibody against H3K9me3 and a negative control IgG antibody. qPCR was performed on two positive control regions (Dazl and MusD (Karimi et al., 2011)) and a negative intergenic control region. The enrichment was calculated over input and represented relative to the intergenic region (Ngondo *et al*, 2018). IgG error bars clipped at axis limit.

(F) Representative Western blots for HP1α in WT, *Ago1*_KO1 and *Ago1*_KO2 mESCs and quantification. * = p value < 0.05 and ns = non-significant, unpaired t-test for n=3 independent experiments.

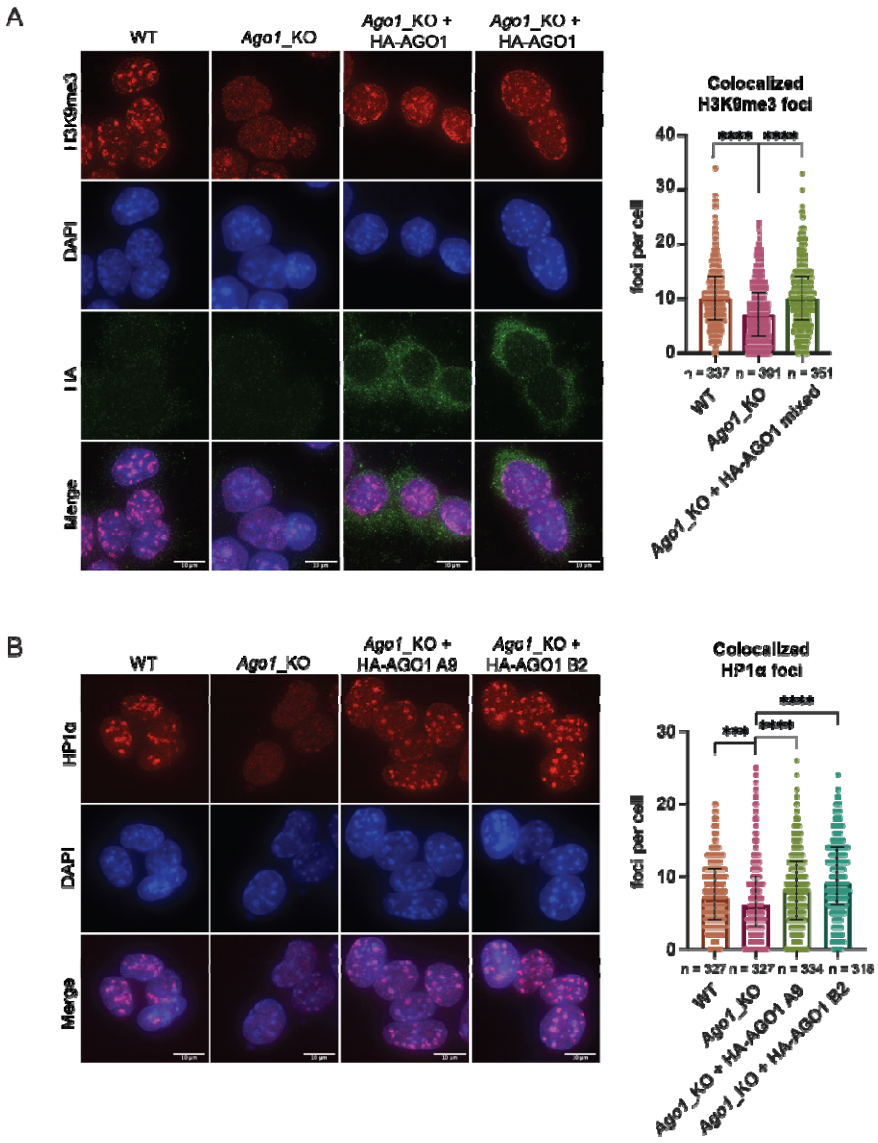

Figure 2. AGO1 complementation rescues the distribution of H3K9me3 and HP1α at pericentromeric regions in *Ago1*_KO mESCs.

(A) Left: Representative IF images of H3K9me3 in WT, *Ago1*_KO and two representative images of *Ago1*_KO + 3x HA-AGO1 mixed population mESCs. scale bar = 10 µm. Right: Quantification of foci count for H3K9me3 that colocalizes with DAPI regions in WT, *Ago1*_KO and *Ago1*_KO + 3x HA-AGO1 mixed population mESCs. The graph shows the median distribution with the interquartile range. **** = p value < 0.0001, Mann-Whitney test for n=3 independent experiments.

(B) Left: Representative IF images of HP1α in WT, *Ago1*_KO and *Ago1*_KO + 3x HA-AGO1 single clones A9 and B2. Right: Quantification of foci count for HP1α that colocalizes with DAPI regions in WT, *Ago1*_KO and *Ago1*_KO + 3x HA-AGO1 single clones A9 and B2. The graph shows the median distribution with the interquartile range. **** = p value < 0.0001, *** = p value < 0.001, Mann-Whitney test for n=3 independent experiments.

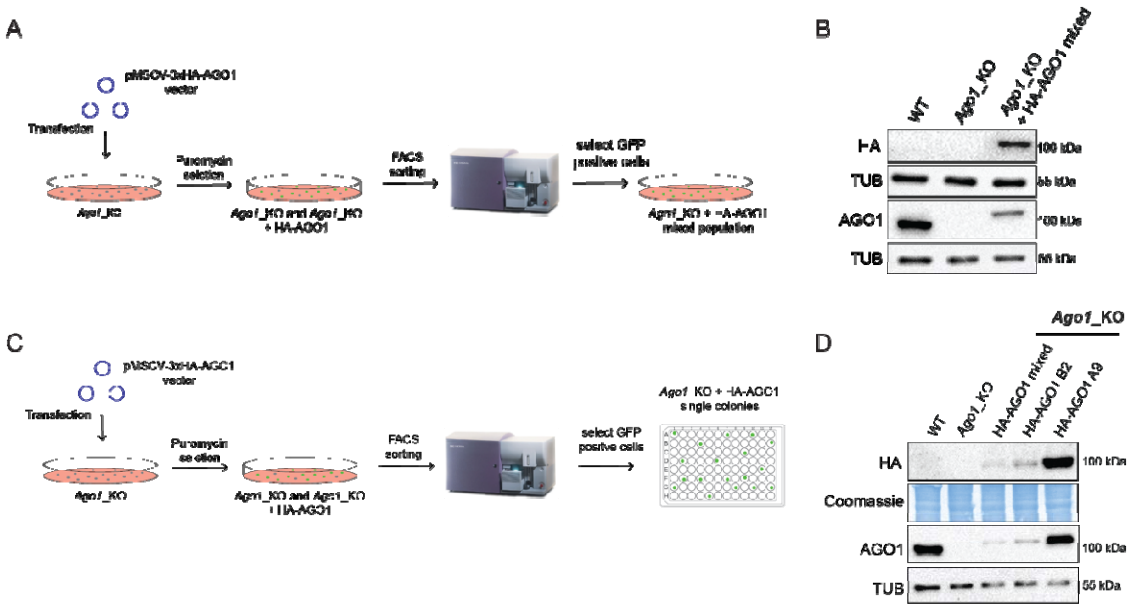

Figure S2. Strategies of the AGO1 rescue experiments.

(A) Schematic representation of the experimental design to reintroduce AGO1 in *Ago1*_KO2 mESCs and select a mixed population.

(B) Representative Western blots for HA and AGO1 in WT, *Ago1*_KO2 and *Ago1*_KO2 + 3x HA-AGO1 mixed population mESCs.

(C) Schematic representation of the experimental design to reintroduce AGO1 in *Ago1*_KO2 mESCs and to select single clones.

(D) Representative Western blots for HA and AGO1 in WT, *Ago1*_KO2 and *Ago1*_KO2 + 3x HA-AGO1 mixed population and the two 3x HA-AGO1 single clones A9 and B2.

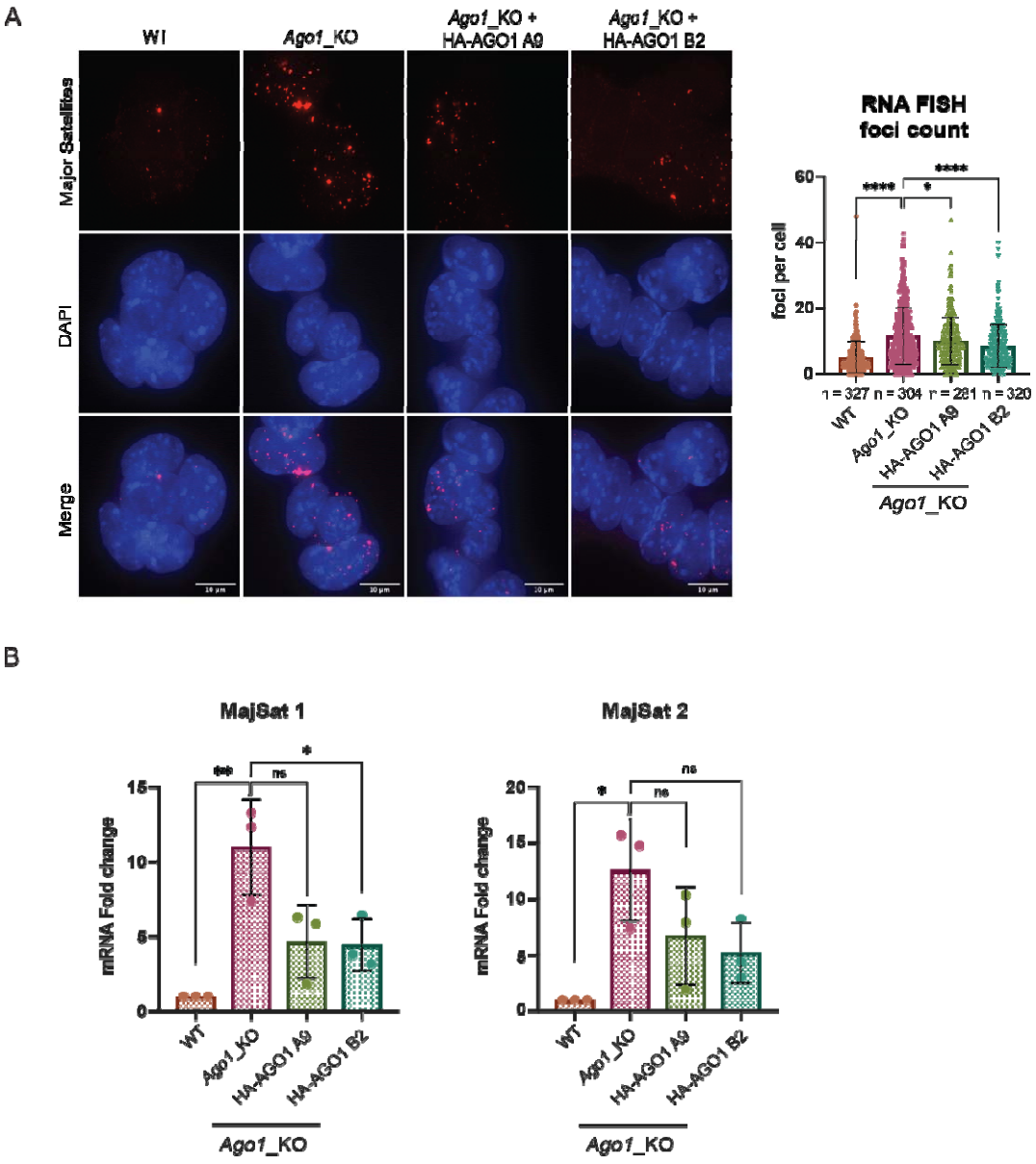

Figure 3. Major satellite transcripts are upregulated in *Ago1*_KO mESCs.

(A) Left: Representative images of major satellite RNA FISH in WT, *Ago1*_KO and two HA-AGO1 single clones, A9 and B2. scale bar = 10 µm. Right: Quantification of Major Satellite RNA FISH foci count in WT and *Ago1*_KO mESCs two HA-AGO1 single clones, A9 and B2. The graph shows the mean distribution with standard deviations. **** = p value < 0.0001 and **** = p value < 0.05 unpaired t-test for n=3 independent experiments.

(B) RT-qPCR results for major satellite primer set 1 and 2 (Table S1) in WT and *Ago1*_KO mESCs and two HA-AGO1 single clones, A9 and B2. * = p value < 0.05 and ** = p value < 0.01, ns = not significant, unpaired t-test for n=3 independent experiments.

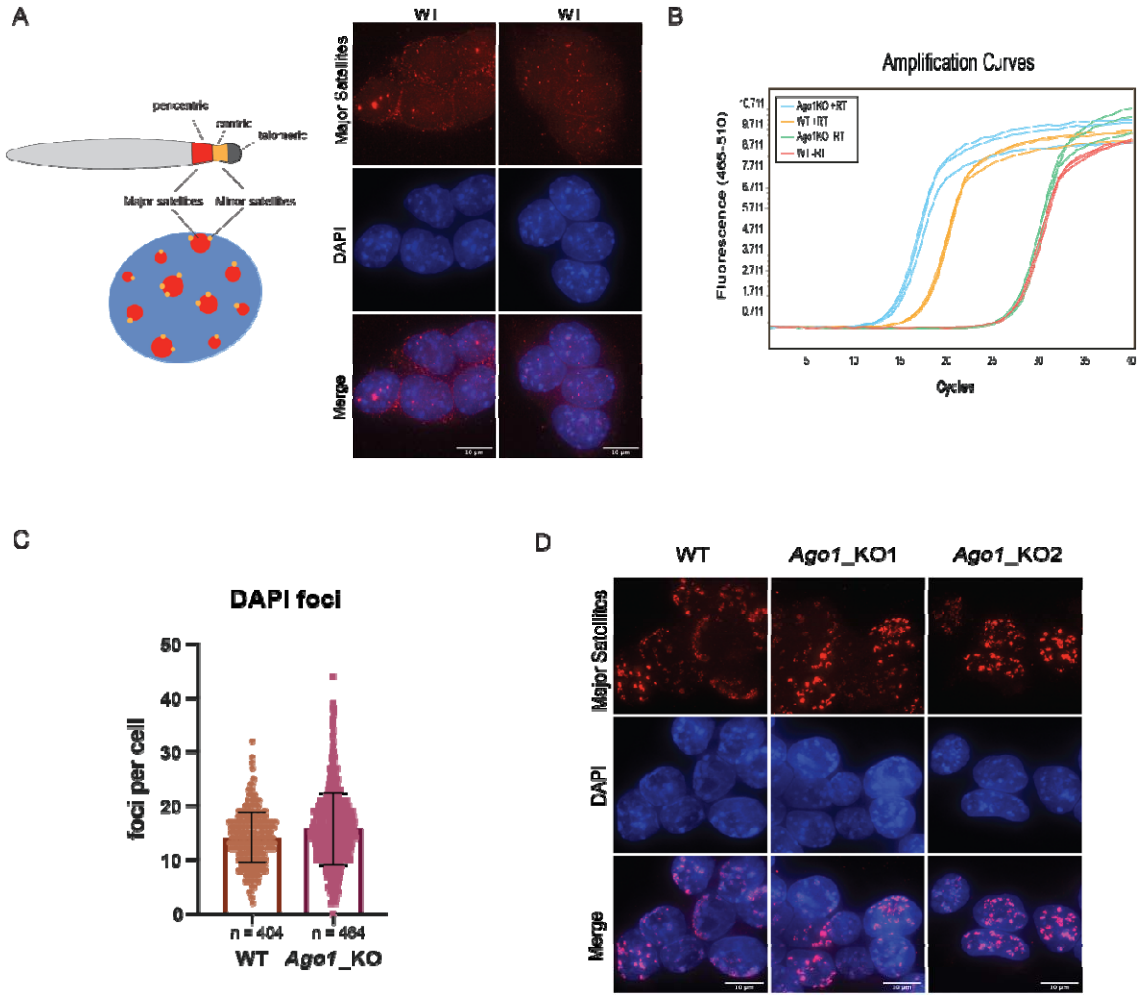

Figure S3. Major satellite transcripts and chromocenter formation.

(A) Schematic representation of mouse pericentromeric regions with major and minor satellites shown in red and orange, respectively. Two representative images of major satellite RNA FISH in WT, showing that major satellite transcripts are detected also in WT mESCs. scale bar = 10 µm.

(B) Amplification curves of WT and *Ago1*_KO qRT-PCR on major satellites in one replicate, showing that the – and + RT are well separated.

(C) Quantification of the DAPI foci count in WT and *Ago1*_KO mESCs. The graph shows the mean distribution with standard deviations.

(D) Representative images of major satellite DNA FISH in WT and *Ago1*_KO mESCs. scale bar = 10 µm.

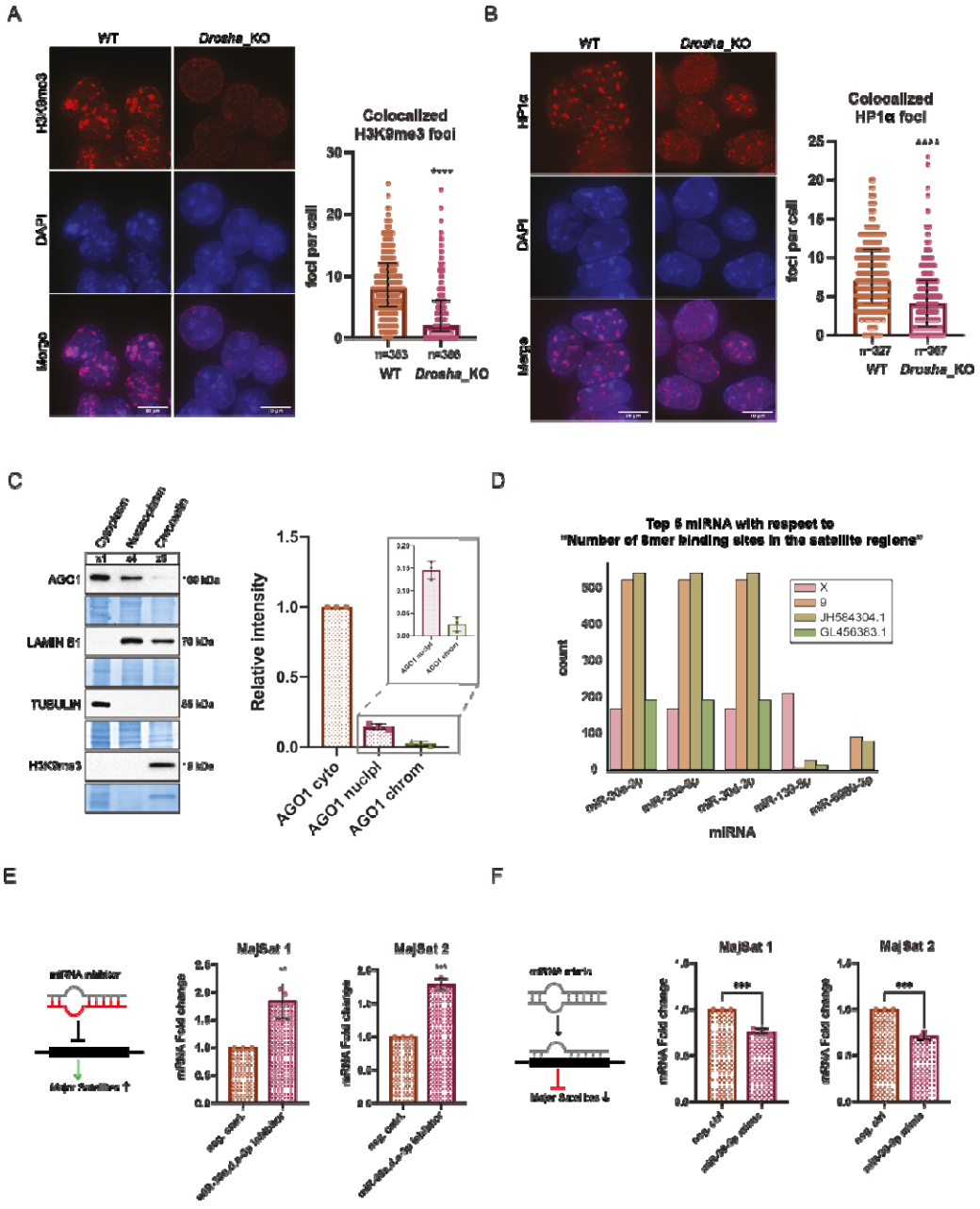

Figure 4. MiRNAs are involved in the regulation of major satellite transcripts

(A) Left: Representative IF images of H3K9me3 in WT and *Drosha*_KO mESCs. scale bar = 10 µm. Right: Quantification of foci count for H3K9me3 that colocalizes with DAPI regions in WT and *Drosha*_KO mESCs. The graph shows the median distribution with the interquartile range. **** = p value < 0.0001, Mann-Whitney test for n=3 independent experiments.

(B) Left: Representative IF images of HP1α in WT and *Drosha*_KO mESCs. Right: Quantification of foci count for HP1α that colocalizes with DAPI regions in WT and *Drosha*_KO mESCs. The graph shows the median distribution with the interquartile range. **** = p value < 0.0001, Mann-Whitney test for n=3 independent experiments.

(C) Representative Western blots for the fractionation of WT mESCs to visualize AGO1 subcellular localization and quantification of n=3 independent experiments. LAMIN B1 (nucleoplasm, chromatin), TUBULIN (cytoplasm), H3K9me3 (chromatin) were used as subcellular markers.

(D) Representation of the top 5 microRNAs with 8mer binding sites targeting major satellite sequences located on chromosomes X, 9 and the genomic contigs JH584304.1 and GL456383.1.

(E) RT-qPCR results for major satellite primer sets 1 and 2 (Table S1) in WT mESCs transfected with a negative control inhibitor and a pool of inhibitors against miR-30a, d, e-3p. ** = p value < 0.01 and *** = p value < 0.001, unpaired t-test for n=3 independent experiments.

(F) RT-qPCR results for major satellite primer sets 1 and 2 (Table S1) in WT mESCs transfected with a negative control mimic and a miR-30-3p mimic. *** = p value < 0.001, unpaired t-test for n=3 independent experiments.

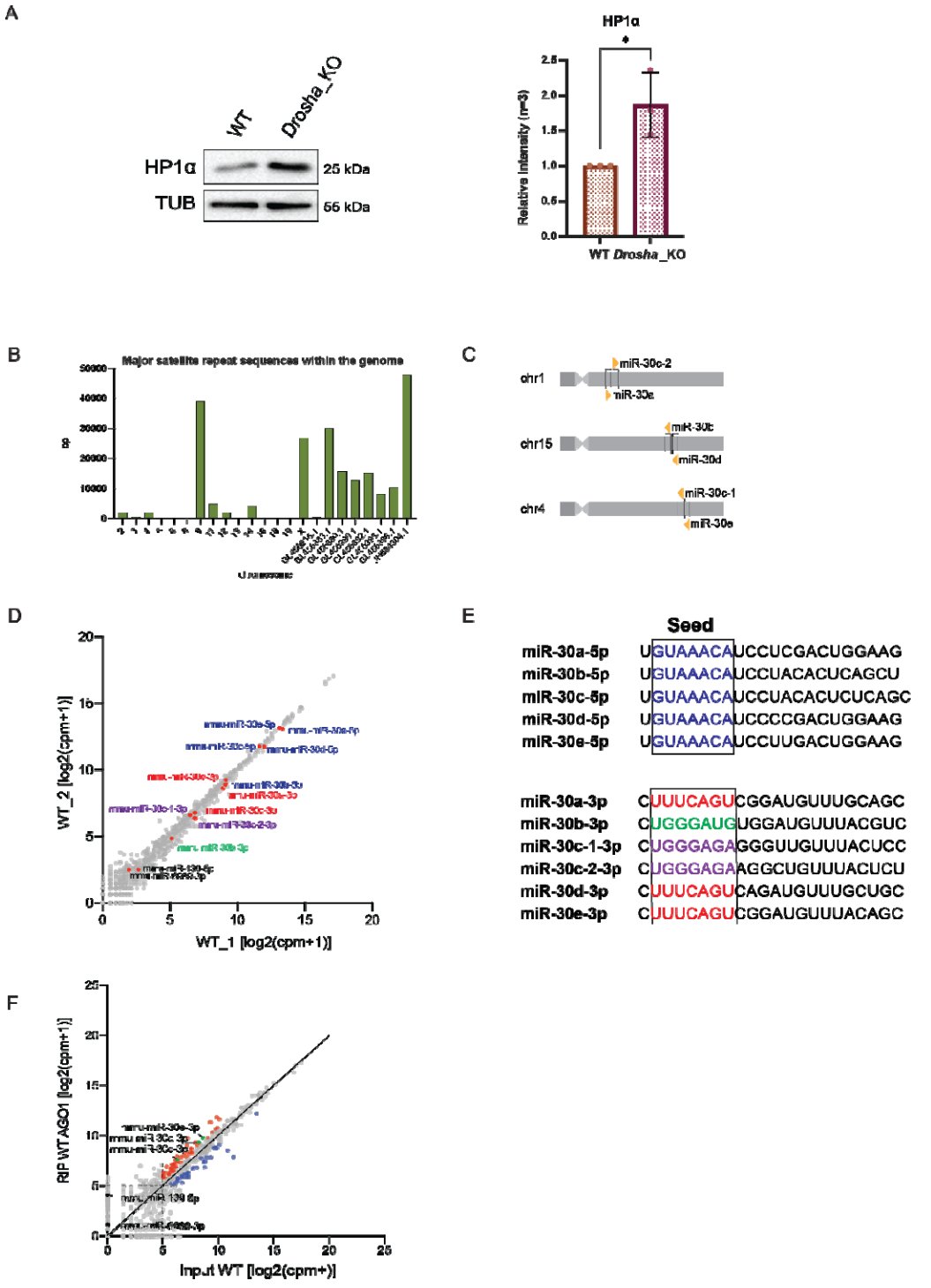

Figure S4. Identification of miRNAs targeting major satellite transcripts.

(A) Representative Western blots for HP1α in WT, *Drosha*_KO. * = p value < 0.05, unpaired t-test for n=3 independent experiments.

(B) Summed length per chromosome or unmapped contig of annotated major satellite sequences within the mouse genome (mm10).

(C) Schematic representation of the miR-30 family in mouse.

(D) Scatterplot showing the log2(cpm+1) of expressed miRNAs in WT mESCs. Highlighted in red are the miR-30a, d, e-3p, in blue the miR-30a, b, c, d, e-5p, in violet miR-30c-1-3p and miR-30c-2-3p and in green miR-30b-3p

(E) Mature miRNA sequences of the miR-30-5p and miR-30-3p's. Highlighted in different colors are the different seed sequences.

(F) Scatterplot showing the log2(cpm+1) counts of miRNAs loaded in AGO1 versus miRNAs expressed in WT mESCs. The top 20% AGO1 loaded miRNAs versus Input with a minimum expression of log2(cpm+1) = 5 are marked in red and the lowest 20% of AGO1 loaded miRNAs versus Input with a minimum expression of log2(cpm+1) = 5 are marked in blue. Highlighted are the miR-30a, d, e-3p.

References of images:

FACS machine in Fig S3: **https://fluorofinder.com/cytometer-facsaria/**

96-well plate: https://commons.wikimedia.org/wiki/File:96-Well_plate.svg